

Photon Correlation Signals in Coupled-Cavity Polaritons Created by Entangled Light

Bing Gu* and Shaul Mukamel*

Cite This: *ACS Photonics* 2022, 9, 938–943

Read Online

ACCESS |



Metrics & More



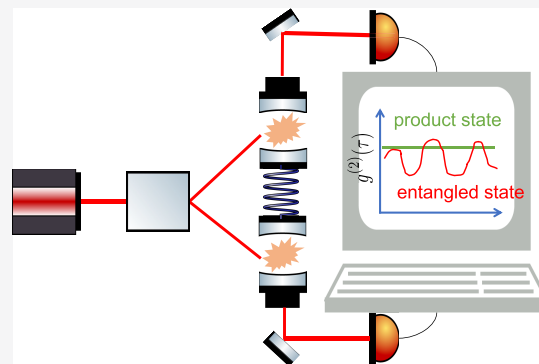
Article Recommendations



Supporting Information

ABSTRACT: We study theoretically a photon-coincidence counting technique aimed at measuring the entanglement between two optical cavities connected by an optical waveguide. Delocalized doubly excited polariton states can be selectively probed by two-photon absorption of an entangled photon pair generated by spontaneous parametric down-conversion with a narrowband pump. Deviations from unity of the second-order correlation function $g^{(2)}(\tau)$ of photons emitted from remote cavities reveal intercavity correlations. The coincidence counting signal in the frequency domain reveals the transition frequencies between single-polariton states and between single polaritons and tripolaritons. High-frequency spectral features arise from the counter-rotating terms in the cavity–molecule coupling, rendering them a direct signature for the ultrastrong coupling regime in cavity quantum electrodynamics.

KEYWORDS: coupled cavity, photon correlation, entangled photon



Optical cavities provide a versatile platform for manipulating the optical, electronic, and chemical properties of embedded materials, as has been demonstrated experimentally and theoretically.^{1–13} Hybrid light–matter states, known as polaritons, emerge in the strong light–matter coupling regime when the cavity–molecule coupling even in the vacuum state becomes stronger than all other decay rates of the system.

Coupled-cavity arrays have found widespread applications in many areas of physics and chemistry. In quantum information science, they offer a promising platform for quantum state transfer¹⁴ and communication.^{15–17} Coupled-cavity networks with the ability to address individual cavities have been proposed as a quantum simulator for strongly coupled many-body systems.^{18,19} In addition, they are widely used for electromagnetically induced transparency²⁰ and slow-light engineering.²¹ By creating delocalized photonic states and multicavity polariton states,^{22–24} coupled cavities with embedded molecules offer a powerful platform for cavity quantum electrodynamics and for the remote control of chemical reactions.²⁵ Such states can be engineered by tuning the cavity frequencies as well as the light–matter and intercavity couplings. Remote cavities can be coupled by optical waveguides. Coupled cavities spanning the entire electromagnetic spectrum from the MHz to X-ray have been realized by photonic crystals²⁶ and Fabry–Perot-type resonators.²⁷

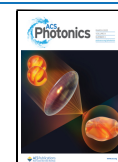
Nonlinear spectroscopy can unveil the interacting polariton states and the correlations between remote cavities. Their single-site addressability on the micron and larger scale allows the design of optical signals with different light beams addressing selected sites. This is not possible within molecular aggregates

with subnanometer molecular separations. Site selectivity can be used to single out Liouville space pathways in the nonlinear response, as has been demonstrated for trapped ion systems.²⁸

Here we study photon correlation measurements in cavity arrays. Photon correlation spectroscopy (PCS) carries matter information via Glauber's photon correlation functions (spatial coordinates are suppressed) $G^{(n)}(t_1, t_2, \dots, t_n) = \langle E^{(-)}(t_1) \dots E^{(-)}(t_n) E^{(+)}(t_n) \dots E^{(+)}(t_1) \rangle$ measured by coincidence counting of n detectors.²⁹ Here $E^{(+)}(t_n)$ and $E^{(-)}(t_n)$ are the positive and negative frequency components of the electric field operator at detector n , respectively. PCS techniques have long been employed to probe cavity polaritons^{30–32} and quantum coherences at non-equilibrium steady states.³³ The proposed technique takes advantage of the single-site addressability of spatially well-separated cavities by photon beams directed at different cavities. Entangled photon pairs generated by spontaneous parametric down-conversion (SPDC) are exploited to excite the coupled cavity to a selected doubly excited polariton eigenstate.^{34,35} By placing a detector outside each cavity and measuring them in coincidence, we demonstrate that the second-order photon correlation function provides a signature of the entanglement of the doubly excited state

Received: November 15, 2021

Published: February 25, 2022



created by entangled two-photon absorption. In the frequency domain, PCS further contains direct spectral signatures of the counter-rotating terms in the cavity–molecule coupling. These terms, which violate the excitation number conservation of the Jaynes–Cummings model,³⁶ are expected to be important in the ultrastrong coupling regime where the light–matter coupling strength becomes comparable to the photon frequency.^{9,37–42} The counter-rotating terms give rise to effects that cannot be explained by resonant interactions such as virtual photons in the joint light–matter ground state^{43,44} and exciting two atoms with a single photon.⁴⁵

In the proposed PCS measurement, sketched in Figure 1, a narrowband pump pulse interacts with a second-order nonlinear

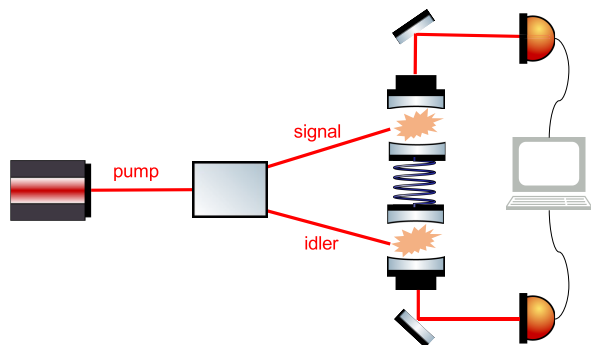


Figure 1. Schematic of the photon correlation signal for a coupled-cavity system. A narrowband laser impinging on the nonlinear crystal generates an entangled photon pair by SPDC. The twin beams enter two well-separated cavities that are connected by an optical waveguide. The photons emitted from the two cavities are measured in coincidence by two photodetectors placed outside each cavity.

crystal, to generate an entangled photon pair, known as signal and idler beams, by a SPDC process. The polariton system consists of molecules embedded in two cavities connected by an optical waveguide. Two-photon absorption (TPA) of the entangled photon pair brings the polariton system from the ground state to a doubly excited state. The system then undergoes a dissipative polariton dynamics where the excitation energy eventually generates an out-of-cavity photon through cavity leakage. The two photon detectors D_1 and D_2 measure photons coming from cavity 1 and 2, respectively.

1. THEORY AND COMPUTATIONAL PROTOCOL

Our setup is described by the Hamiltonian ($\hbar = 1$)

$$H = H_M + H_{CM} + H_{CC} + H_{CE} + H_E + H_R + H_{RM} \quad (1)$$

Here

$$H_M = \sum_{j=1}^2 \sum_{n=1}^N \epsilon_j \sigma_{jn}^\dagger \sigma_{jn} \quad (2)$$

describes N identical two-level systems with transition frequencies ϵ_j embedded in the j th cavity and $\sigma_{jn} = |e_{jn}\rangle\langle g_{jn}|$, $|g_{jn}\rangle$ ($|e_{jn}\rangle$) is the ground (excited) state of the n th molecule in the j th cavity with the transition dipole operator $\mu_{jn} = \sigma_{jn}^\dagger + \sigma_{jn}$. The incoming entangled signal and idler beams generated by SPDC are described by the Hamiltonian

$$H_R = \int_0^\infty d\omega \omega (a_s^\dagger(\omega) a_s(\omega) + a_i^\dagger(\omega) a_i(\omega)) \quad (3)$$

and interact with the embedded molecules via $H_{RM} = \sum_n -\mu_{1n} \cdot E_s(\mathbf{r}_{1n}) - \mu_{2n} \cdot E_i(\mathbf{r}_{2n})$. The electric field operator of the signal/idler beam, directed into cavity 1/2, reads $E_{s/i}(\mathbf{r}) = i \int_0^\infty d\omega \mathcal{E}(\omega) a_{s/i} \mathbf{e}_{s/i} e^{i\mathbf{k} \cdot \mathbf{r}} + \text{H.c.}$, where $\mathcal{E}(\omega) = \sqrt{\hbar\omega/2\epsilon_0 n A}$ is the single-photon electric field, A is the quantization area, $\mathbf{e}_{s/i}$ is the signal/idler beam polarization, and n is the refraction index.⁴⁶ The coupled-cavity Hamiltonian H_{CC} describes the two cavities and the connecting optical waveguide. When the waveguide modes are off-resonant from the two cavities, they can be eliminated, leading to an effective cavity Hamiltonian

$$H_{CC} = \omega_1 a_1^\dagger a_2 + \omega_2 a_2^\dagger a_1 - J(a_1 a_2^\dagger + a_1^\dagger a_2) \quad (4)$$

where J is the effective intercavity hopping strength and ω_j the j th cavity frequency.⁴⁷ $J = 1$ –10 meV has been demonstrated for photonic crystal cavities.^{26,48} The detectors measure the extracavity modes $b_j(\omega)$, described by H_E , which are bilinearly coupled to the cavity modes through H_{CE} , leading to cavity loss; see section S2.

The intracavity light–matter interaction in the electric dipole approximation reads

$$H_{CM} = \sum_j \sum_n -ig_j (\sigma_{jn} + \sigma_{jn}^\dagger) (a_j - a_j^\dagger) \quad (5)$$

where $g_j = \mathcal{E}(\omega_j) \langle e_{jn} | \mu_{jn} \cdot \mathbf{e}_j | g_{jn} \rangle$ and \mathbf{e}_j is the j th cavity mode polarization. Note that we have not invoked the rotating wave approximation (RWA) and thus retain the counter-rotating terms $\sigma a + \sigma^\dagger a^\dagger$. Despite their small influence on the energy levels, they lead to unique spectral features in the PCS, as will be shown below.

We focus on the parameter regime where the cavity–molecule coupling is stronger than the photon hopping, which is in turn larger than the cavity decay rate, i.e., $g \gg J \gg \kappa$. It then makes sense to use the isolated cavity as the starting point for our analysis. For brevity, we suppress the cavity index while discussing the single-cavity polaritons. In the strong coupling regime, the light–matter interaction creates hybrid light–matter polariton states, that are linear combinations of molecular and cavity-excited states. It is instructive to consider the polariton states under the RWA even though it is not invoked in the simulations. The bright state is created by the collective exciton operator $X^\dagger |G\rangle$ with $X^\dagger = 1/\sqrt{N} \sum_n \sigma_{n}^\dagger$, where $|G\rangle = |g\rangle \otimes |0\rangle$ is the joint cavity–matter ground state under RWA. The intracavity polariton operator

$$P_\mu^\dagger = \alpha_\mu X^\dagger + \beta_\mu a^\dagger \quad (6)$$

$\mu = \pm$, creates a polaritonic excitation. The polariton operators in general do not satisfy the boson commutation relations because the excitons are not bosons. However, in some cases the exciton operators can be approximately taken as bosons. Equation 6 can be inverted to give $a_j = \sum_\mu \gamma_\mu^{(j)} P_\mu$. The intercavity coupling can then be recast as $J(a_1 a_2^\dagger + \text{H.c.}) = J_{\mu\nu} \sum_{\mu,\nu} P_\mu^{(1)} P_\nu^{(2)\dagger} + \text{H.c.}$, where $J_{\mu\nu} = J \gamma_\mu^{(1)} \gamma_\nu^{*(2)}$. Thus, photon hopping can also be viewed as polariton hopping.

Employing an entangled photon pair allows the simultaneous excitation of both cavities. Using a narrowband pump, one can selectively excite a desired delocalized bipolariton eigenstate via a TPA process, even though the signal and idler beams are broadband. Similar spectral resolution can be achieved with classical continuous wave lasers, but it is then not possible to control the excitation time of the two cavities. In contrast, with a

short entanglement time, entangled photons excite both cavities simultaneously, thus defining the zero time for the coincidence measurement. The SPDC-generated twin-photon state is given in section S6.

By sending the signal and idler beams into different cavities, we can selectively prepare bipolariton states where both cavities are excited, thus excluding doubly excited states in a single cavity. The two-photon-excited coupled-cavity state is created by two dipole interactions in different cavities. Note that the entangled photons are used as an actinic pulse; the coincidence measurement reveals interpolariton correlations in the prepared eigenstate rather than in the photon pair.

The normalized PCS is defined by the coincidence counting rate of D_1 and D_2

$$g^{(2)}(\tau) = \frac{G^{(2)}(\tau)}{\langle b_2^\dagger(\tau)b_2(\tau) \rangle \langle b_1^\dagger b_1 \rangle} \quad (7)$$

where $\langle \dots \rangle \equiv \text{Tr}\{\rho \dots\}$, with ρ being the density matrix of the entire system. Here $G^{(2)}(\tau) = \langle b_1^\dagger b_2^\dagger(\tau)b_2(\tau)b_1(\tau) \rangle$, where $b_j(t) \propto E_j^{(+)}(t)$ is the Heisenberg picture extracavity electric field operator at detector D_j , measures the joint probability of detecting photon 1 at time 0 and photon 2 at time τ .

According to the input–output theory,^{38,49} the electric field operators outside and inside the cavity are linked by (see section S2)

$$b_j(z, t) = b_j^0(t - z/c) + \sqrt{\kappa_j} a_j(t - z/c) \quad (8)$$

for $j = 1, 2$, where b_j^0 is a free field and κ_j is the j th cavity decay rate. Here we assume that cavity leak is the main decay channel because the cavity lifetime is typically shorter than that of the molecular excitations. Inserting eq 8 into eq 7 yields

$$g^{(2)}(\tau) = \frac{\langle a_1^\dagger a_2^\dagger(\tau) a_2(\tau) a_1(\tau) \rangle_f}{\langle a_2^\dagger(\tau) a_2(\tau) \rangle_f \langle a_1^\dagger a_1 \rangle_f} \quad (9)$$

where τ is the time difference between two detection events and $\langle \dots \rangle_f = \text{Tr}\{\rho_f \dots\}$, where $\rho_f = |f\rangle\langle f|$ is the initial bipolariton state selectively excited by the entangled photon pair. We had computed eq 9 by solving the quantum master equation

$$\dot{\rho}_t = \mathcal{L}\rho_t = -i[H_0, \rho_t] + \sum_{j=1}^2 \kappa_j \mathcal{D}[a_j]\rho_t \quad (10)$$

where ρ_t is the joint cavity + molecule density matrix, $H_0 = H_M + H_{MC} + H_{CC}$, and $\mathcal{D}[a]\rho = a\rho a^\dagger - \frac{1}{2}\{a^\dagger a, \rho\}$ is the Lindblad superoperator describing the cavity leakage; see section S1 for computational details.

2. RESULTS AND DISCUSSION

Figure 2 shows the PCS for two nonidentical cavities of four states created by entangled photons for different intercavity coupling strength. At $J = 0$, the four states reduce to product states $|5\rangle_{J=0} = |P_-P_- \rangle \equiv |P_-^{(1)} \rangle \otimes |P_-^{(2)} \rangle$, $|8\rangle_{J=0} = |P_-P_+ \rangle$, $|9\rangle_{J=0} = |P_+P_- \rangle$, $|12\rangle_{J=0} = |P_+P_+ \rangle$. The eigenstates are numbered from low to high energy. At $J \neq 0$, these states can be qualitatively different due to mixing of states close in energy. We assumed a single molecule $N = 1$ in each cavity, thus neglecting contributions from collective dark states.⁵⁰ The doubly excited intracavity polariton states for $N = 1$ and $N \gg 1$ are also different,⁵¹ but these states cannot be effectively excited in our setup.

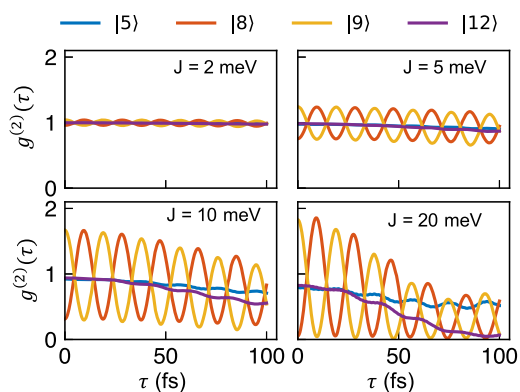


Figure 2. Second-order photon correlation function $g^{(2)}(\tau)$ (eq 9) for two coupled cavities with different initially excited states and with different intercavity couplings J as indicated. The coupled-cavity eigenstates are numbered from low to high energies. The correlation function is computed by eq 10, as detailed in the Supporting Information. $N = 1$, $\epsilon_1 = 1.02$ eV, $\epsilon_2 = 1.005$ eV, $\omega_1 = 1.02$ eV, $\omega_2 = 1.008$ eV, $g_1 = g_2 = 108.8$ meV.

At zero delay, $g^{(2)}(0)$ reveals whether the prepared state is a product or entangled. For a product state, $G^{(2)}(0) = \langle a_2^\dagger a_2 \rangle \langle a_1^\dagger a_1 \rangle$ and hence $g^{(2)}(0) = 1$. For entangled states, a Schmidt decomposition can be used

$$|f\rangle = \sum_{\alpha} \sqrt{\lambda_{\alpha}} |\phi_{\alpha}\rangle |\chi_{\alpha}\rangle \quad (11)$$

where λ_{α} are the Schmidt coefficients $\sum_{\alpha} \lambda_{\alpha} = 1$ and $|\phi_{\alpha}\rangle$, $|\chi_{\alpha}\rangle$ are the Schmidt modes. Substituting eq 11 into eq 9 yields

$$g^{(2)}(0) = \frac{\sum_{\alpha, \beta} \sqrt{\lambda_{\alpha} \lambda_{\beta}} \langle \phi_{\beta} | N_1 | \phi_{\alpha} \rangle \langle \chi_{\beta} | N_2 | \chi_{\alpha} \rangle}{\left(\sum_{\alpha} \lambda_{\alpha} \langle \phi_{\alpha} | N_1 | \phi_{\alpha} \rangle \right) \left(\sum_{\beta} \lambda_{\beta} \langle \chi_{\beta} | N_2 | \chi_{\beta} \rangle \right)} \quad (12)$$

where $N_1 = a_1^\dagger a_1$ and $N_2 = a_2^\dagger a_2$. In general, eq 12 will not equal to unity.

For vanishing intercavity coupling $J = 0$, we have

$$g^{(2)}(\tau) = 1 \quad (13)$$

This is because, for a product state $|f\rangle = |P_{\mu}P_{\nu}\rangle$, the two cavities are uncoupled upon the two-photon excitation and remain so during the ensuing dissipative dynamics. The second-order correlation function can then be factorized, $G^{(2)}(\tau) = \langle a_2^\dagger(\tau) a_2(\tau) \rangle \langle a_1^\dagger a_1 \rangle$, resulting in eq 13.

The deviation of $g^{(2)}(\tau)$ from unity is a direct measure of intercavity correlations. Due to polariton hopping, the doubly excited state $|f\rangle$ is a linear combination of the single-polariton product states $|P_{\mu}P_{\nu}\rangle$, which may further mix with intracavity bipolariton states. When state $|f\rangle$ is an entangled state of the two cavities, $g^{(2)}(\tau) \neq 1$. As shown in Figure 2, states $|8\rangle$ and $|9\rangle$ exhibit strong oscillations during the time delay between the two detection events, which increase with J , meaning that these two states become highly entangled upon turning on the intercavity coupling. This can be rationalized that since the two product states $|P_-P_+ \rangle$ and $|P_+P_- \rangle$ are close in energy and are coupled through the photon hopping, the eigenstates for $J \neq 0$ are mixtures of these two states. In contrast, states $|5\rangle$ and $|12\rangle$ are less entangled as their $g^{(2)}(\tau)$ remains close to 1. This implies that the product states $|P_-P_- \rangle$ and $|P_+P_+ \rangle$ are not sensitive to photon hopping. This is expected, as their energy is separated from the other two states by a Rabi energy. Figure 2 shows that the PCS signal acts as a direct indicator of correlations in the

doubly excited state. The correlation between remote cavities is encoded in the correlation of the emitted photons. This is not the case if one cannot distinguish between the sources of emitted photons (cf. Dicke super-radiance⁵²).

For identical cavities, the states $|P_+P_-\rangle$ and $|P_-P_+\rangle$ are degenerate. Even for $J = 0$, entangled photons can create entangled polariton states that are an equal mixture of these two states because the signal and idler beams can be spectrally broad and cover both the upper and lower polariton states $|P_\pm\rangle$. The emitted photons in this case are also correlated, resulting in $g^{(2)} \neq 1$ similar to Figure 2, and their intercavity correlation can then be detected. This does not occur for classical light because classical sources cannot create entangled states. Hence, the emitted photons from classical excitation always have $g^{(2)}(\tau) = 1$.

Apart from revealing the correlation between different cavities, the PCS signal provides a unique signature for the counter-rotating terms in the cavity–molecule coupling. There are also counter-rotating terms in the intercavity coupling, but their effects on the spectrum are much weaker. A better understanding of the PCS signal can be achieved by rewriting the unnormalized $G^{(2)}(\tau)$ in the form

$$G^{(2)}(\tau) = \text{Tr}\{a_2\mathcal{G}(\tau)\{a_1\rho_0a_1^\dagger\}a_2^\dagger\} \quad (14)$$

The Liouville space time-evolution operator $\mathcal{G}(\tau) = e^{\mathcal{L}\tau}$ contains the eigenvalues of the Liouvillian superoperator \mathcal{L} (eq 10). The $a_1\rho_0a_1^\dagger$ in eq 14 can be understood as the system density matrix after observing photon 1 at time 0, $\mathcal{G}(\tau)$ represents a free time evolution for τ , and $a_2\dots a_2^\dagger$ represents photon 2 being detected.

If bath effects can be simply described by a decay of the coherence (i.e., pure dephasing),

$$\mathcal{L}|ij\rangle\rangle = \Omega_{ij}|ij\rangle\rangle \quad (15)$$

where $|ij\rangle\rangle$ is the Liouville space representation of $|i\rangle\langle j|$ (see section S4 for the transformation from Hilbert space to Liouville space) and $\Omega_{ij} = -i\omega_{ij} - \gamma_{ij}$ with $\omega_{ij} = \omega_i - \omega_j$ being the transition frequency between the system eigenstates $|i\rangle$ and $|j\rangle$ and γ_{ij} the decay rate of coherence $|ij\rangle\rangle$. The Fourier transform of the time-domain signal then reveals the transition frequencies of the entire polariton system. A typical $G^{(2)}(\omega)$, shown in Figure 3, exhibits features in two spectral regions. The strong low-frequency region (\sim Rabi frequency Ω_R) corresponds to the transition frequencies between single-polariton states. This feature can be interpreted using the ladder diagram (i) in Figure 4a, which represents one Liouville space pathway contributing to the correlation function in eq 14. The four yellow interactions represent the TPA process, whereas the upper four interactions represent the two-photon detection process. Upon two-photon excitation, the entire system is in the population state $|ff\rangle\rangle$ where the bipolariton state $|f\rangle$ is selected by the pump frequency. The photon detection in D_1 is represented by two outgoing arrows, which can bring the system into a coherence $|e_i e_j\rangle\rangle$ between single-polariton states $|e_i\rangle$. This coherence oscillates in time with frequency $\omega_{e_i e_j}$ which is close to the Rabi frequency and thus creates features in the low-frequency regime.

The relatively weak high-frequency features match the transition energies between the bipolariton states and the ground state. It turns out, however, that these peaks come from the transitions between the single polaritons and the tripolariton manifold, states with eigenenergies around triple the cavity frequencies $3\omega_c$. These features can be attributed to a non-RWA process whereby the cavity changes from a bipolariton to a

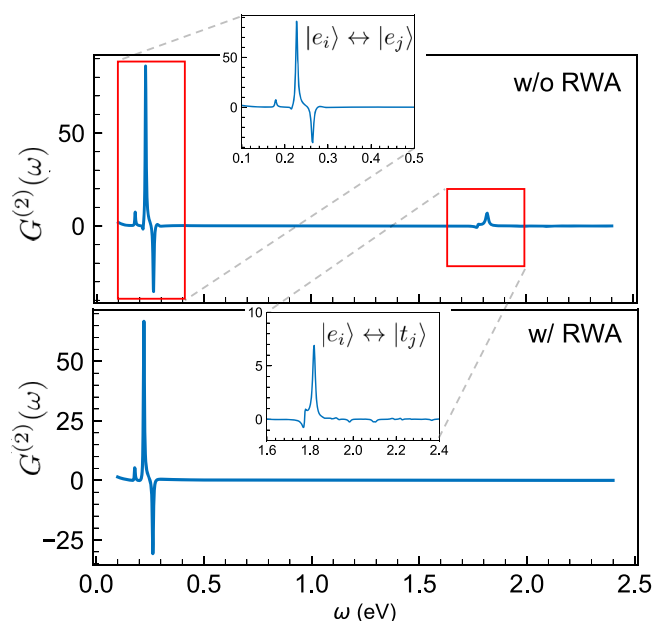


Figure 3. Fourier transform of the second-order photon correlation signal $G^{(2)}(\omega)$ (eq 14) for initial state $|S\rangle$. The two insets are zoomed-in images of the two spectral regions. Here $J = 40$ meV, where the other parameters are the same as Figure 2.

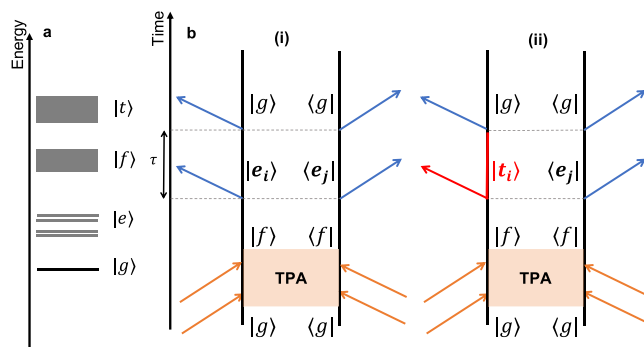


Figure 4. Ladder diagrams representing the correlation function in eq 14. (a) Level scheme of the coupled-cavity system. (b) Diagrams i and ii correspond to the low-frequency and high-frequency regions, respectively, of the signal in Figure 3. The transition marked in red in diagram ii represents a non-RWA process whereby the polariton emits a photon and goes to the higher excited state.

tripolariton state while emitting a photon. This process can be represented by diagram ii in Figure 4, where the non-RWA process is marked in red. To verify the physical origin of the high-frequency features in the signal, we confirmed that the high-frequency regime disappears if the RWA is invoked for the cavity–matter coupling; see the lower panel of Figure 3.

3. CONCLUSIONS

We have calculated the photon correlation signal from two remote cavities with entangled photon excitation. The frequency anticorrelation of the entangled photon pair allows the bipolariton eigenstates to be resolved, and the temporal correlation allows both cavities to be excited simultaneously. In the time domain, this signal reveals entanglement in the doubly excited states involving both cavities. Noninteracting cavities result in a normalized photon correlation function $g^{(2)}(\tau) = 1$. In the frequency domain, the signal contains features

in two spectral regions: the low-frequency region reveals transition frequencies between single-polariton states, whereas the high-frequency region reveals the transitions between the single polariton and tripolariton states. The high-frequency features arise from the counter-rotating terms in the cavity–molecule coupling even when the coupling strength does not reach the ultrastrong coupling regime. The present signal can be extended to an array of coupled cavities (quantum network¹⁶) and measure the correlation functions between remote cavities that are not directly coupled.

■ ASSOCIATED CONTENT


SI Supporting Information

The Supporting Information is available free of charge at <https://pubs.acs.org/doi/10.1021/acsphotonics.1c01755>.

Computational details; input–output relations; expressing correlation functions in terms of eigenstates of the Liouvillian superoperator; rules to transform from Hilbert to Liouville space; and SPDC-created twin-photon state (PDF)

■ AUTHOR INFORMATION

Corresponding Authors

Bing Gu – Department of Chemistry and Department of Physics & Astronomy, University of California, Irvine, California 92697, United States;  orcid.org/0000-0002-5787-3334; Email: bingg@uci.edu

Shaul Mukamel – Department of Chemistry and Department of Physics & Astronomy, University of California, Irvine, California 92697, United States;  orcid.org/0000-0002-6015-3135; Email: smukamel@uci.edu

Complete contact information is available at: <https://pubs.acs.org/10.1021/acsphotonics.1c01755>

Notes

The authors declare no competing financial interest.

■ ACKNOWLEDGMENTS

We thank Dr. Feng Chen for inspiring discussions. This work is supported by the National Science Foundation Grant CHE-1953045. The work of S.M. was supported by the U.S. Department of Energy, Office of Science, Office of Basic Energy Sciences under Award Number DE-SC0022134.

■ REFERENCES

- (1) Thomas, A.; Lethuillier-Karl, L.; Nagarajan, K.; Vergauwe, R. M. A.; George, J.; Chervy, T.; Shalabney, A.; Devaux, E.; Genet, C.; Moran, J.; Ebbesen, T. W. Tilting a Ground-State Reactivity Landscape by Vibrational Strong Coupling. *Science* **2019**, *363*, 615–619.
- (2) Ebbesen, T. W. Hybrid Light–Matter States in a Molecular and Material Science Perspective. *Acc. Chem. Res.* **2016**, *49*, 2403–2412.
- (3) Ribeiro, R. F.; Martínez-Martínez, L. A.; Du, M.; Campos-Gonzalez-Angulo, J.; Yuen-Zhou, J. Polariton Chemistry: Controlling Molecular Dynamics with Optical Cavities. *Chem. Sci.* **2018**, *9*, 6325–6339.
- (4) Herrera, F.; Owrutsky, J. Molecular Polaritons for Controlling Chemistry with Quantum Optics. *J. Chem. Phys.* **2020**, *152*, 100902.
- (5) Gu, B.; Mukamel, S. Cooperative Conical Intersection Dynamics of Two Pyrazine Molecules in an Optical Cavity. *J. Phys. Chem. Lett.* **2020**, *11*, 5555–5562.
- (6) Gu, B.; Nenov, A.; Segatta, F.; Garavelli, M.; Mukamel, S. Manipulating Core Excitations in Molecules by X-Ray Cavities. *Phys. Rev. Lett.* **2021**, *126*, No. 053201.
- (7) Gu, B.; Mukamel, S. Optical-Cavity Manipulation of Conical Intersections and Singlet Fission in Pentacene Dimers. *J. Phys. Chem. Lett.* **2021**, *12*, 2052–2056.
- (8) Gu, B.; Mukamel, S. Manipulating Nonadiabatic Conical Intersection Dynamics by Optical Cavities. *Chem. Sci.* **2020**, *11*, 1290–1298.
- (9) Forn-Díaz, P.; Lamata, L.; Rico, E.; Kono, J.; Solano, E. Ultrastrong Coupling Regimes of Light–Matter Interaction. *Rev. Mod. Phys.* **2019**, *91*, No. 025005.
- (10) Chikkaraddy, R.; de Nijs, B.; Benz, F.; Barrow, S. J.; Scherman, O. A.; Rosta, E.; Demetriadou, A.; Fox, P.; Hess, O.; Baumberg, J. J. Single-Molecule Strong Coupling at Room Temperature in Plasmonic Nanocavities. *Nature* **2016**, *535*, 127–130.
- (11) Herrera, F.; Spano, F. C. Cavity-Controlled Chemistry in Molecular Ensembles. *Phys. Rev. Lett.* **2016**, *116*, 238301.
- (12) Hirai, K.; Hutchison, J. A.; Uji-i, H. Recent Progress in Vibropolaritonic Chemistry. *ChemPlusChem.* **2020**, *85*, 1981–1988.
- (13) Feist, J.; Galego, J.; Garcia-Vidal, F. J. Polaritonic Chemistry with Organic Molecules. *ACS Photonics* **2018**, *5*, 205–216.
- (14) Cirac, J.; Zoller, P.; Kimble, H.; Mabuchi, H. Quantum State Transfer and Entanglement Distribution among Distant Nodes in a Quantum Network. *Phys. Rev. Lett.* **1997**, *78*, 3221–3224.
- (15) van Enk, S. J.; Kimble, H. J.; Cirac, J. I.; Zoller, P. Quantum Communication with Dark Photons. *Phys. Rev. A* **1999**, *59*, 2659–2664.
- (16) Ritter, S.; Nölleke, C.; Hahn, C.; Reiserer, A.; Neuzner, A.; Uphoff, M.; Mücke, M.; Figueroa, E.; Bochmann, J.; Rempe, G. An Elementary Quantum Network of Single Atoms in Optical Cavities. *Nature* **2012**, *484*, 195–200.
- (17) Kimble, H. J. The Quantum Internet. *Nature* **2008**, *453*, 1023–1030.
- (18) Greentree, A. D.; Tahan, C.; Cole, J. H.; Hollenberg, L. C. L. Quantum Phase Transitions of Light. *Nature Phys.* **2006**, *2*, 856–861.
- (19) Hartmann, M. J.; Brandao, F. G. S. L.; Plenio, M. B. Strongly Interacting Polaritons in Coupled Arrays of Cavities. *Nat. Phys.* **2006**, *2*, 849–855.
- (20) Liu, Y.-C.; Li, B.-B.; Xiao, Y.-F. Electromagnetically Induced Transparency in Optical Microcavities. *Nanophotonics* **2017**, *6*, 789–811.
- (21) Yariv, A.; Xu, Y.; Lee, R. K.; Scherer, A. Coupled-Resonator Optical Waveguide: A Proposal and Analysis. *Opt. Lett.* **1999**, *24*, 711–713.
- (22) Lin, G. W.; Zou, X. B.; Lin, X. M.; Guo, G. C. Scalable, High-Speed One-Way Quantum Computer in Coupled-Cavity Arrays. *Appl. Phys. Lett.* **2009**, *95*, 224102.
- (23) Kato, S.; Némethy, N.; Senga, K.; Mizukami, S.; Huang, X.; Parkins, S.; Aoki, T. Observation of Dressed States of Distant Atoms with Delocalized Photons in Coupled-Cavities Quantum Electrodynamics. *Nat. Commun.* **2019**, *10*, 1160.
- (24) Xiang, B.; Wang, J.; Yang, Z.; Xiong, W. Nonlinear Infrared Polaritonic Interaction between Cavities Mediated by Molecular Vibrations at Ultrafast Time Scale. *Sci. Adv.* **2021**, *7*, No. eabf6397.
- (25) Du, M.; Ribeiro, R. F.; Yuen-Zhou, J. Remote Control of Chemistry in Optical Cavities. *Chem.* **2019**, *5*, 1167–1181.
- (26) Majumdar, A.; Rundquist, A.; Bajcsy, M.; Dasika, V. D.; Bank, S. R.; Vučković, J. Design and Analysis of Photonic Crystal Coupled Cavity Arrays for Quantum Simulation. *Phys. Rev. B* **2012**, *86*, 195312.
- (27) Haber, J.; Kong, X.; Strohm, C.; Willing, S.; Gollwitzer, J.; Bocklage, L.; Ruffer, R.; Pálffy, A.; Röhlberger, R. Rabi Oscillations of X-ray Radiation between Two Nuclear Ensembles. *Nat. Photonics* **2017**, *11*, 720–725.
- (28) Blatt, R.; Roos, C. F. Quantum Simulations with Trapped Ions. *Nature Phys.* **2012**, *8*, 277–284.
- (29) Glauber, R. J. *Quantum Theory of Optical Coherence*; John Wiley & Sons, Ltd: 2006; pp 23–182.
- (30) Dorfman, K. E.; Mukamel, S. Indistinguishability and Correlations of Photons Generated by Quantum Emitters Undergoing Spectral Diffusion. *Sci. Rep.* **2015**, *4*, 3996.

- (31) Dorfman, K. E.; Schlawin, F.; Mukamel, S. Nonlinear Optical Signals and Spectroscopy with Quantum Light. *Rev. Mod. Phys.* **2016**, *88*, No. 045008.
- (32) Dorfman, K. E.; Mukamel, S. Multidimensional Photon Correlation Spectroscopy of Cavity Polaritons. *Proc. Natl. Acad. Sci. U. S. A.* **2018**, *115*, 1451–1456.
- (33) Sánchez Muñoz, C.; Schlawin, F. Photon Correlation Spectroscopy as a Witness for Quantum Coherence. *Phys. Rev. Lett.* **2020**, *124*, 203601.
- (34) Rubin, M. H.; Klyshko, D. N.; Shih, Y. H.; Sergienko, A. V. Theory of Two-Photon Entanglement in Type-II Optical Parametric down-Conversion. *Phys. Rev. A* **1994**, *50*, 5122–5133.
- (35) Couteau, C. Spontaneous Parametric Down-Conversion. *Contemporary Physics* **2018**, *59*, 291–304.
- (36) Shore, B. W.; Knight, P. L. Topical Review: The Jaynes-Cummings Model. *J. Mod. Opt.* **1993**, *40*, 1195–1238.
- (37) Frisk Kockum, A.; Miranowicz, A.; De Liberato, S.; Savasta, S.; Nori, F. Ultrastrong Coupling between Light and Matter. *Nat. Rev. Phys.* **2019**, *1*, 19–40.
- (38) Ciuti, C.; Carusotto, I. Input-Output Theory of Cavities in the Ultrastrong Coupling Regime: The Case of Time-Independent Cavity Parameters. *Phys. Rev. A* **2006**, *74*, No. 033811.
- (39) Gambino, S.; Mazzeo, M.; Genco, A.; Di Stefano, O.; Savasta, S.; Patanè, S.; Ballarini, D.; Mangione, F.; Lerario, G.; Sanvitto, D.; Gigli, G. Exploring Light–Matter Interaction Phenomena under Ultrastrong Coupling Regime. *ACS Photonics* **2014**, *1*, 1042–1048.
- (40) Garziano, L.; Ridolfo, A.; De Liberato, S.; Savasta, S. Cavity QED in the Ultrastrong Coupling Regime: Photon Bunching from the Emission of Individual Dressed Qubits. *ACS Photonics* **2017**, *4*, 2345–2351.
- (41) Garziano, L.; Ridolfo, A.; Stassi, R.; Di Stefano, O.; Savasta, S. Switching on and off of Ultrastrong Light-Matter Interaction: Photon Statistics of Quantum Vacuum Radiation. *Phys. Rev. A* **2013**, *88*, No. 063829.
- (42) Anappara, A. A.; De Liberato, S.; Tredicucci, A.; Ciuti, C.; Biasiol, G.; Sorba, L.; Beltram, F. Signatures of the Ultrastrong Light-Matter Coupling Regime. *Phys. Rev. B* **2009**, *79*, 201303.
- (43) De Liberato, S. Virtual Photons in the Ground State of a Dissipative System. *Nat. Commun.* **2017**, *8*, 1465.
- (44) Stassi, R.; Ridolfo, A.; Di Stefano, O.; Hartmann, M. J.; Savasta, S. Spontaneous Conversion from Virtual to Real Photons in the Ultrastrong-Coupling Regime. *Phys. Rev. Lett.* **2013**, *110*, 243601.
- (45) Garziano, L.; Macrì, V.; Stassi, R.; Di Stefano, O.; Nori, F.; Savasta, S. One Photon Can Simultaneously Excite Two or More Atoms. *Phys. Rev. Lett.* **2016**, *117*, No. 043601.
- (46) Blow, K. J.; Loudon, R.; Phoenix, S. J. D.; Shepherd, T. J. Continuum Fields in Quantum Optics. *Phys. Rev. A* **1990**, *42*, 4102–4114.
- (47) Sato, Y.; Tanaka, Y.; Upham, J.; Takahashi, Y.; Asano, T.; Noda, S. Strong Coupling between Distant Photonic Nanocavities and Its Dynamic Control. *Nat. Photonics* **2012**, *6*, 56–61.
- (48) Cai, T.; Bose, R.; Solomon, G. S.; Waks, E. Controlled Coupling of Photonic Crystal Cavities Using Photochromic Tuning. *Appl. Phys. Lett.* **2013**, *102*, 141118.
- (49) Gardiner, C. W.; Collett, M. J. Input and Output in Damped Quantum Systems: Quantum Stochastic Differential Equations and the Master Equation. *Phys. Rev. A* **1985**, *31*, 3761–3774.
- (50) Ribeiro, R. F.; Martínez-Martínez, L. A.; Du, M.; Campos-Gonzalez-Angulo, J.; Yuen-Zhou, J. Polariton Chemistry: Controlling Molecular Dynamics with Optical Cavities. *Chem. Sci.* **2018**, *9*, 6325–6339.
- (51) Gu, B.; Mukamel, S. Manipulating Two-Photon-Absorption of Cavity Polaritons by Entangled Light. *J. Phys. Chem. Lett.* **2020**, *11*, 8177–8182.
- (52) Dicke, R. H. Coherence in Spontaneous Radiation Processes. *Phys. Rev.* **1954**, *93*, 99–110.

Supporting Information: Photon-Correlation Signals in Coupled-Cavity Polaritons Created by Entangled Light

Bing Gu^{1,*} and Shaul Mukamel^{1,†}

¹*Department of Chemistry and Department of Physics & Astronomy,
University of California, Irvine, CA 92697, USA*

CONTENTS

S1. Computational details	S1
S2. Initial Two-Photon Excitation	S1
S3. Cavity leakage	S2
S4. Correlation function computed by diagonalizing the Liouvillian	S3
S5. Transformation From Hilbert space to Liouville space	S3
S6. Twin-photon state	S4
References	S4

S1. COMPUTATIONAL DETAILS

The polariton space is constructed by a direct product of the Hilbert space for each molecule and each cavity, i.e., $|\alpha n \beta m\rangle \equiv |\alpha\rangle \otimes |n\rangle \otimes |\beta\rangle \otimes |m\rangle$, $\alpha, \beta = g, e$ and $n, m = 0, 1, 2, \dots$. The Fock space for each cavity is truncated at 4, i.e., the maximum number state considered is $|3\rangle$. The correlation function is computed by directly diagonalizing the Liouvillian superoperator, detailed in Sec. S4. The parameters used in the computations are $\epsilon_1 = 1.02$ eV, $\epsilon_2 = 1.005$ eV, $\omega_1 = 1.002$ eV, $\omega_2 = 1.05$ eV, $g_1 = g_2 = 0.004$ a.u., the cavity quality factors $Q_1 = Q_2 = 400$.

S2. INITIAL TWO-PHOTON EXCITATION

The final state of the coupled cavity after the entangled two-photon absorption reads

$$|f\rangle = \int_{t_0}^{\infty} dt' \int_{t_0}^t dt' V_s^\dagger(t) V_i^\dagger(t') |G\rangle \times \langle 0| E_s^{(+)}(t) E_i^{(+)}(t') |\Phi\rangle + (s \leftrightarrow i). \quad (\text{S1})$$

where $V_j(t)$ ($V_j^\dagger(t)$) is the dipole lowering (raising) operator in the interaction picture of $H_0 = H_M + H_{MC} + H_{CC}$ is obtained by two dipole couplings in each cavity where $V_j(t)$ ($V_j^\dagger(t)$) is the dipole lowering (raising) operator in the interaction picture of $H_0 = H_M + H_{MC} + H_{CC}$ is obtained by two dipole couplings in each cavity.

In contrast, the classical two-photon absorption with two cw lasers reads

$$T_{fg} = E_s E_i \int_{-\infty}^{\infty} dt \int_{-\infty}^t dt' \langle f | V_s^\dagger(t) V_i^\dagger(t') | g \rangle e^{-i\omega_s t} e^{-i\omega_i t'} + (s \leftrightarrow i) \\ = \delta(\omega_{fg} - \omega_s - \omega_i) \left(\sum_e \frac{\mu_{fe}^{(s)} \mu_{eg}^{(i)}}{\omega_{eg} - \omega_i} \right) \quad (\text{S2})$$

* bingg@uci.edu

† smukamel@uci.edu

where E_j is the electric field amplitude for j beam.

S3. CAVITY LEAKAGE

The electric field operator outside the optical cavity can be obtained from the input-output relations [1] connecting the input and output field operators. For convenience, we consider a simplified model of a one-sided optical cavity with the Hamiltonian given by

$$H = \omega_c a^\dagger a + \int_0^\infty d\omega \omega b^\dagger(\omega) b(\omega) + H_{\text{int}} \quad (\text{S3})$$

where $b(\omega), b^\dagger(\omega)$ are the annihilation and creation operators of the (outgoing) extracavity modes satisfying $[b(\omega), b^\dagger(\omega)] = \delta(\omega - \omega')$, and H_{int} describes the interaction between intracavity and extracavity modes.

The electric field operator reads

$$E^{(+)}(z, t) = i \int_0^\infty d\omega \mathcal{E}(\omega) b(\omega) e^{i\omega(t-z/c)} \approx i \mathcal{E}(\Omega) e^{-i\Omega(t-z/c)} \int_{-\infty}^{+\infty} d\omega b(\omega) e^{-i\omega(t-z/c)} \quad (\text{S4})$$

where in the last step we have assumed the relevant modes are centered at the carrier frequency Ω (e.g. the cavity mode frequency), and also extended the range of integration to $-\infty$ by changing the variable $\omega \rightarrow \omega + \Omega$. It is useful to define the field operator

$$b(z, t) = e^{i\Omega(t-z/c)} \int_{-\infty}^{+\infty} d\omega b(\omega) e^{-i\omega(t-z/c)}, \quad (\text{S5})$$

then the number operator $n(z, t) = \langle b^\dagger(z, t) b(z, t) \rangle$ determines the photon count rate (in units of s^{-1}) at spacetime point (z, t) .

The interaction between intracavity and extracavity modes is given by

$$H_{\text{int}} = i \int_{-\infty}^{+\infty} d\omega g(\omega) b^\dagger(\omega) a + \text{H.c.} \quad (\text{S6})$$

The Heisenberg equation of motion for the extracavity field operator is

$$\dot{b}(\omega, t) = -i\omega b(\omega, t) + g(\omega) a(t) \quad (\text{S7})$$

The solution to Eq. (S7) reads

$$b(\omega, t) = b_0(\omega) e^{-i\omega(t-t_0)} + g(\omega) \int_{t_0}^t e^{-i\omega(t-t')} a(t') dt' \quad (\text{S8})$$

where $b_0(\omega) = b(\omega, t_0)$.

$$b_{\text{out}}(z, t) = \int_{-\infty}^{+\infty} \frac{d\omega}{\sqrt{2\pi}} b(\omega, t) e^{i\omega z/c} \quad (\text{S9})$$

and inserting Eq. (S8) into Eq. (S9) leads to

$$b_{\text{out}}(z, t) = b_{\text{in}}(t) + \int_{-\infty}^{+\infty} \frac{d\omega}{\sqrt{2\pi}} g(\omega) \int_{t_0}^t dt' e^{-i\omega(t-t'-z/c)} a(t') dt' \quad (\text{S10})$$

where the input field is defined as

$$b_{\text{in}}(t) = \int_{-\infty}^{+\infty} \frac{d\omega}{\sqrt{2\pi}} b_0(\omega) e^{-i\omega(t-t_0)} \quad (\text{S11})$$

Assuming a flat spectral density $g^2(\omega) = \kappa/2\pi$, Eq. (S10) reduces to

$$b_{\text{out}}(z, t) = b_{\text{in}}(t - z/c) + \sqrt{\kappa} a(t - z/c) \quad (\text{S12})$$

S4. CORRELATION FUNCTION COMPUTED BY DIAGONALIZING THE LIOUVILLIAN

Here we show how to compute the multitime correlation function in terms of the right and left eigenstates of the Liouvillian. The basic rules transforming from Hilbert space to Liouville space is shown in Sec. S5.

Assuming the time-independent Liouvillian \mathcal{L} is diagonalizable

$$\mathcal{L}|\mu\rangle\rangle = \Omega_\mu|\mu\rangle\rangle, \quad \mathcal{L}^\dagger|\Phi'_\mu\rangle\rangle = \Omega_\mu^*|\Phi'_\mu\rangle\rangle \quad (\text{S13})$$

where $|\Phi_\alpha\rangle\rangle$ and $|\Phi'_\alpha\rangle\rangle$ are, respectively, the right and left eigenvectors, and

$$\Omega_\mu = -i\omega_\mu - \gamma_\mu \quad (\text{S14})$$

are the complex eigenvalues. The eigenvalues and right- and left-eigenvectors completely determine the dissipative quantum dynamics, i.e., the propagator in the Liouville space,

$$\mathcal{G}(t) = \sum_\mu e^{\Omega_\mu t} \frac{|\Phi_\alpha\rangle\rangle\langle\langle\Phi'_\alpha|}{\langle\langle\Phi'_\alpha|\Phi_\alpha\rangle\rangle}. \quad (\text{S15})$$

The many-point correlation functions can be expressed in terms of the complex eigenvalues and eigenstates. For two-point correlation functions, denoting ρ_0 as the initial density matrix, it reads

$$\text{Tr} \{A(t)B\rho_0\} = \frac{\langle\langle A^\dagger|\Phi_\alpha\rangle\rangle\langle\langle\Phi'_\alpha|B\rho_0\rangle\rangle}{\langle\langle\Phi'_\alpha|\Phi_\alpha\rangle\rangle} e^{\Omega_\mu t} \quad (\text{S16})$$

where A, B are arbitrary operators. For three-point correlation functions,

$$\langle A(t)B(t+\tau)C(t) \rangle = \langle\langle \mathbf{I}|\mathcal{B}_L\mathcal{U}(\tau)\mathcal{A}_R\mathcal{C}_L\mathcal{U}(t)|\rho_0 \rangle\rangle = \sum_{\alpha,\beta} e^{\Omega_\beta\tau + \Omega_\alpha t} \frac{\langle\langle \mathbf{I}|\mathcal{B}_L|\Phi_\beta \rangle\rangle\langle\langle\Phi'_\beta|\mathcal{A}_R\mathcal{C}_L|\Phi_\alpha \rangle\rangle\langle\langle\Phi'_\alpha|\rho_0 \rangle\rangle}{\langle\langle\Phi'_\alpha|\Phi_\alpha \rangle\rangle\langle\langle\Phi'_\beta|\Phi_\beta \rangle\rangle} \quad (\text{S17})$$

where $\mathcal{O}_L\rho = \mathcal{O}\rho$, $\mathcal{O}_R\rho = \rho\mathcal{O}$ are the left and right superoperators. The correlation function expressed using superoperators can be conveniently represented by a ladder diagram [2].

S5. TRANSFORMATION FROM HILBERT SPACE TO LIOUVILLE SPACE

Some useful relations are listed below for transforming simulations from Hilbert space to Liouville space. Inner product in the Liouville space

$$\text{Tr} \{A^\dagger B\} \rightarrow \langle\langle A|B \rangle\rangle \quad (\text{S18})$$

Trace of a density matrix leads to

$$\text{Tr} \{\rho\} \rightarrow \langle\langle \mathbf{I}|\rho \rangle\rangle \quad (\text{S19})$$

For an observable represented by operator A in the Hilbert space

$$\text{Tr} \{A\rho\} = \frac{1}{2}\text{Tr} \{\mathcal{A}_+\rho\} = \frac{1}{2}\langle\langle \mathbf{I}|\mathcal{A}_+|\rho \rangle\rangle = \langle\langle \mathbf{I}|\mathcal{A}_L|\rho \rangle\rangle \quad (\text{S20})$$

$$\text{Tr} \{\mathcal{A}_-\rho\} = 0 \quad (\text{S21})$$

For commutators

$$\langle[A, B]\rangle = \frac{1}{2}\langle\langle \mathbf{I}|\mathcal{A}_+\mathcal{B}_-|\rho \rangle\rangle \quad (\text{S22})$$

The linear response function reads

$$\chi = \langle[V(t), V]\rangle = \frac{1}{2}\text{Tr} \{\mathcal{V}_+(t)\mathcal{V}_-\rho_0\} = \frac{1}{2}\langle\langle \mathbf{I}|\mathcal{V}_+(t)\mathcal{V}_-|\rho_0 \rangle\rangle \quad (\text{S23})$$

S6. TWIN-PHOTON STATE

The state of the signal-idler photon pair is given by

$$|\Phi\rangle = \iint d\omega_s d\omega_i \Phi(\omega_s, \omega_i) a_s^\dagger(\omega_s) a_i^\dagger(\omega_i) |0\rangle \quad (\text{S24})$$

where $\Phi = A_p(\omega_s + \omega_i)\phi(\omega_s, \omega_i)$ is the joint spectral amplitude, $A_p(\omega_s + \omega_i)$ the pump spectral envelope, and $\phi(\omega_s, \omega_i)$ the phase-matching function. For a narrowband pulse, $A_p(\omega_s + \omega_i) \propto \delta(\omega_s + \omega_i - \omega_p)$, and the phase-matching function reduces to

$$\phi(\omega_s, \omega_i) \propto \text{sinc}(\Delta_s T_e / 2) \quad (\text{S25})$$

with the entanglement time T_e , $\Delta_s = \omega_s - \bar{\omega}_s$ is the deviation from the central frequency and $\Delta_i = -\Delta_s$ [3, 4].

-
- [1] C. W. Gardiner and M. J. Collett, Input and output in damped quantum systems: Quantum stochastic differential equations and the master equation, *Phys. Rev. A* **31**, 3761 (1985).
 - [2] S. Mukamel, *Principles of Nonlinear Optical Spectroscopy* (Oxford University Press, 1995).
 - [3] B. Gu and S. Mukamel, Manipulating Two-Photon-Absorption of Cavity Polaritons by Entangled Light, *J. Phys. Chem. Lett.* **11**, 8177 (2020).
 - [4] M. H. Rubin, Transverse correlation in optical spontaneous parametric down-conversion, *Phys. Rev. A* **54**, 5349 (1996).